Analysis of the Compliance Properties of an Industrial Robot with the Mozzi Axis Approach

Alberto Doria [1], **Silvio Cocuzza** [1,*], **Nicola Comand** [2], **Matteo Bottin** [2] **and Aldo Rossi** [1]

1   Department of Industrial Engineering, University of Padova, 35131 Padova, Italy;
    alberto.doria@unipd.it (A.D.); aldo.rossi@unipd.it (A.R.)
2   Department of Management and Engineering, University of Padova, 36100 Vicenza, Italy;
    nicola.comand@phd.unipd.it (N.C.); matteo.bottin.1@phd.unipd.it (M.B.)
*   Correspondence: silvio.cocuzza@unipd.it; Tel.: +39-049-827-6793

Abstract: In robotic processes, the compliance of the robot arm plays a very important role. In some conditions, for example, in robotic assembly, robot arm compliance can compensate for small position and orientation errors of the end-effector. In other processes, like machining, robot compliance may generate chatter vibrations with an impairment in the quality of the machined surface. In industrial robots, the compliance of the end-effector is chiefly due to joint compliances. In this paper, joint compliances of a serial six-joint industrial robot are identified with a novel modal method making use of specific modes of vibration dominated by the compliance of only one joint. Then, in order to represent the effect of the identified compliances on robot performance in an intuitive and geometric way, a novel kinematic method based on the concept of "Mozzi axis" of the end-effector is presented and discussed.

Keywords: robot; compliance; machining; modal testing; Mozzi axis

1. Introduction

The compliance properties of industrial robots are very important for many industrial applications, such as automatic robotic assembly and material removal processes (e.g., machining and deburring). On the one hand, in robotic assembly, joint compliance can be useful for compensating dimensional errors in the parts to be assembled; on the other hand, in material removal processes, a low Cartesian compliance (high stiffness) of the end-effector is required. Indeed, still very few robots have been applied in this economically important application area [1] mainly due to their low stiffness. Moreover, the compliance properties of robots appear very important in emerging fields such as flexible assembly systems [2,3] and collaborative robotics [4].

From a static point of view, low stiffness causes imprecise products, due to the robot deflections during the robotic task. From a dynamic point of view, low frequency chatter vibrations [5–7] can be induced when low-stiffness robots are used, with an impairment in the quality of the machined surface. Moreover, induced vibrations cause a reduction of tool life and can damage robot joint transmission.

In particular, the low joint stiffness of the robot is one of the main issues in using robotic machining instead of CNC machining. Indeed, it is well established in the literature (see, for example, [8]) that the dominant contribution factor for a large displacement of the robot end-effector is joint compliance (mainly due to gear transmission elasticity), while link flexibility can be neglected. Moreover, the stiffness of an industrial robot is usually on the level of 10^6 N/m (with a base natural frequency of robot around 10 Hz), while a standard CNC machine has stiffness on the level of 10^8 N/m (with a base natural frequency of several hundred Hz or even more than 1000 Hz) [5]. Sometimes, combinations of serial and parallel kinematic chains have been proposed to increase robot stiffness [9].

The static force/torque-deformation experiments and identification are widely used to obtain the joint stiffness of industrial robots with good accuracy [10]. During the static experiments, a set of forces/torques is applied to the robot end-effector (or to a single joint) in different robot configurations, while the displacement sensors (e.g., vision system, CMM, or laser sensors) measure the steady-state deformation of the end-effector. Therefore, the Cartesian stiffness of the robot can be calculated. Then, through the analytical relation between the joint and Cartesian stiffness based on the kinematic model of robot, many types of identification methods (e.g., least squares or genetic algorithms) can be employed to obtain the joint stiffness. Most of the works in the literature (e.g., see [8,11–14]) neglect link flexibility and identify the joints' rotational stiffness (modeled with linear rotational springs) using this method. In [15], the robotic arm is modeled considering rigid links and three lumped rotational springs for each joint to take into account joint compliance, bearings compliance, and link deflections, which are all identified with the above method. In [16], an analysis approach in which both joint and link stiffness are considered is presented.

It is worth mentioning that in [13], the identified joint stiffnesses are then used in an analytical model, in which natural frequencies and mode shapes are validated through modal testing experiments. In particular, a good match is demonstrated between the first two experimental natural frequencies and related mode shapes and the corresponding ones predicted by the analytical model.

In [17], experimental modal analysis is used to identify the joint and base stiffness of an industrial robot represented with a four-degrees-of-freedom (four-DOF) planar model.

In robotic processes, the directions along which the robot arm is compliant are very important. The stiffness matrix in the joint space does not directly give this information; moreover, for a serial robot, the stiffness matrix in the Cartesian space is not diagonal and it is configuration-dependent. This means that the force and deformation in the Cartesian space are coupled (e.g., a force applied in one direction will cause a deformation in all possible directions) and this can generate some counter-intuitive results. Moreover, due to the difference in compliance in different directions, machining accuracy can be different in different directions.

Since the end-effector of the robot, which is grasping a tool or an object, can be considered a rigid body mounted on the compliant robot, the basic ideas of the screw theory [18] can be adopted to describe its motion.

In this paper, first, a novel method for the identification of robot stiffness is presented (Section 2). It is based on the selective excitation of modes of vibration that chiefly involve only one joint. Since in this specific case modal stiffness coincides with joint stiffness, the latter can be identified from the measured natural frequency and the calculated value of moment of inertia. A serial six-DOF robot is considered (Omron Adept Viper s650), since it is representative of industrial robots used for a wide range of operations. Then, a new method for representing linear and rotational compliance using the concept of screw or Mozzi axis is presented (Section 3). The proposed method is a useful tool to understand how the robot deforms with respect to the working surface, and to highlight the joints that give the largest contribution to robot compliance in specific configurations. Furthermore, robot configurations that place the Mozzi axis in the most favorable position with respect to the working surface can be found. Finally, the compliance properties of the tested robot are analyzed with the proposed method in different robot configurations (Section 4), and conclusions are drawn.

2. Identification

2.1. Testing Equipment and Method

Stiffness (or compliance) properties of robot joints are usually measured by means of static tests [13] carrying out measurements in the Cartesian space. Then, a mathematical model is used to

correlate force vector {*F*} and deformation vector {Δx} in Cartesian space with the stiffness matrix $\left[K_q \right]$ in the joint space. $\left[K_q \right]$ is diagonal and the following equation holds [8]:

$$\{\Delta x\} = [J(q)]\left[K_q\right]^{-1}[J(q)]^T\{F\} \tag{1}$$

where $[J(q)]$ is the Jacobian matrix that depends on robot configuration. Matrix $\left[K_q \right]$ can be obtained from Equation (1) by least-square method considering some different configurations of the robot [8,13].

In this paper, a different approach based on modal testing is adopted. The basic idea is to excite modes of vibration dominated by the compliance of one joint and to identify stiffness (or compliance) from the measured modal frequency and the moment of inertia about the joint axis. The moment of inertia is calculated by means of the CAD (Computer Aided Design) model of the robot.

The equipment needed to carry out this kind of test is rather simple and cheap; it includes a hammer for modal testing, an accelerometer, and a data acquisition board. In the framework of this research, a PCB 086C01 hammer (with load cell sensitivity 0.2549 mV/N), a PCB 356A17 triaxial accelerometer (sensitivity 50.5 mV/(m/s^2)) built by PCB Piezotronics, Inc., Depew, NY, USA, and a NI9234 data acquisition board were used built by National Instruments, Austin, TX, USA. After some preliminary tests, a sampling frequency of 1024 Hz and 2048 samples were selected. Measured signals were analyzed by means of ModalVIEW R2, a specific software for modal analysis.

Since motions of the base of the robot may have a negative effect on the quality of measurements, the robot was rigidly fastened to a large steel base (see Figure 1) and an accelerometer was used to monitor residual base motions.
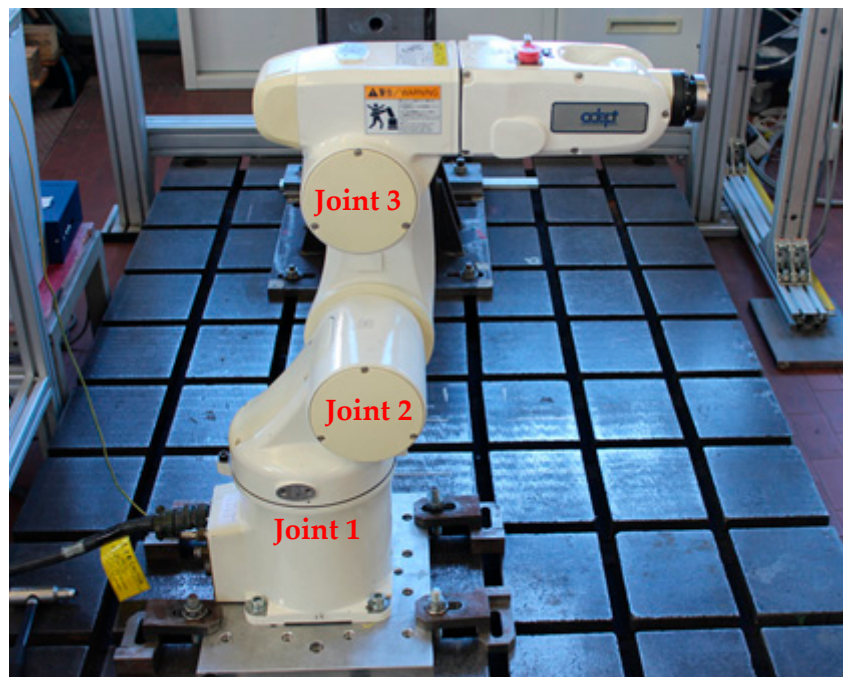
Figure 1. The robot in the testing rig.

When a serial six-joint robot is loaded by a force applied on the end-effector, on the one hand, this force produces the largest moments about the first joints, and on the other hand, the rotations of the first joints due to compliance have the largest effect on end-effector positioning errors, due to the large lever arms [19]. For these reasons, the present research is limited to the identification of the compliance properties of the first three joints of the robot. The last three joints are considered ideal revolute joints that contribute to define the pose of the end-effector, but are infinitely stiff. In the future,

the method will be used to identify the compliance of all the joints, if the compliance of the wrist joints will appear relevant in some configurations.

Since in actual working conditions the joints of the robot are held in the desired configuration by the servomotors, the tests were carried out with the servomotors switched on. The identified stiffnesses are the result of the mechanical stiffness of the transmission plus the stiffness of the servo.

In order to identify the stiffnesses of the first three joints of the robot, three specific test conditions were defined (see Table 1). The first condition, which is represented in Figure 2, aimed to highlight the stiffness of the first joint. For this reason, the end-effector flange was excited by a lateral force (y direction) and joint rotations were set in order to achieve the maximum arm extension. In this configuration, the first mode of vibration should be dominated by the compliance of the first joint.
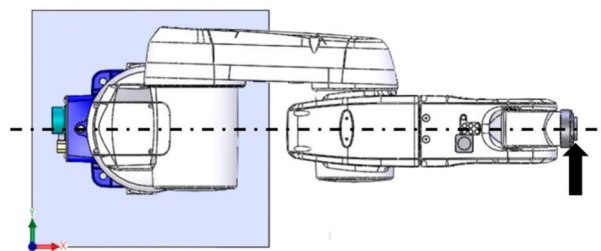

Figure 2. Test configuration 1 for the identification of the stiffness of joint 1.

Table 1. Robot configurations.

Configuration	Joint 1 [°]	Joint 2 [°]	Joint 3 [°]	Joint 4 [°]	Joint 5 [°]	Joint 6 [°]
Test 1	0	0	90	0	0	0
Test 2	0	0	16.96	0	−16.96	0
Test 3	0	−37.54	176.73	0	49.20	0
Validation	0	30	30	0	0	0

The second test condition (Figure 3) aimed to highlight the stiffness of joint 2. For this reason, the robot arm was configured with the approach axis of the end-effector pointing upwards and intersecting the axis of joint 3, and a vertical force was exerted by the hammer. Since in this test configuration the impact force intersected the axis of joint 3 and was parallel to the axis of joint 1, the compliances of these joints should not have influenced the fundamental mode of vibration.
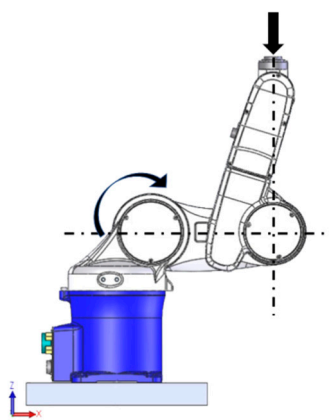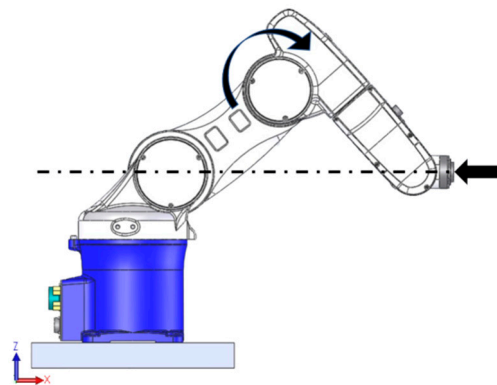

Figure 3. Test configuration 2 for the identification of the stiffness of joint 2.

Figure 4 shows the third test configuration. In this case, the approach axis of the end-effector was aligned to the x axis and intersected both the axis of joint 2 and the axis of joint 1. Therefore,

the fundamental mode of vibration excited by a hammer force in x direction should have been dominated by the stiffness of joint 3.

Figure 4. Test configuration 3 for the identification of the stiffness of joint 3.

The tests were carried out with the modal analysis approach [20], which is widely used in the fields of automotive engineering [21,22], aerospace engineering [23], automatic machines [24], and robotics [25]. A grid of measurement points was defined on the robot (see Figure 5); points 10 and 11 were used to monitor base vibrations. In each test configuration, the hammer impact was always exerted on the end-effector flange in the defined direction, whereas the triaxial accelerometer was moved to the various grid points (rowing response approach). In this way, for each configuration, 33 frequency response functions (FRFs) were measured between the 3 acceleration components of the 11 grid points and the hammer impact force. In order to improve the repeatability and quality of measurements, each FRF was calculated averaging the results obtained with three hammer blows. Measured data were then processed with ModalVIEW in order to identify natural frequencies, modal dampings, and modal shapes.

(**a**)   (**b**)
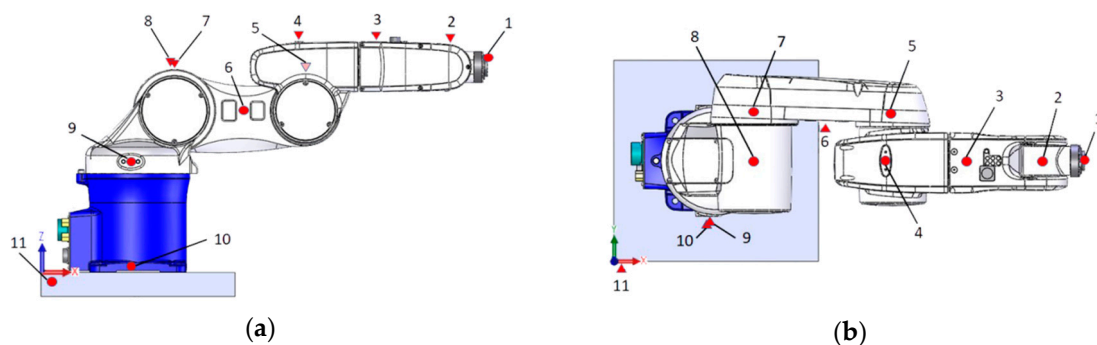
Figure 5. Set of measurement points: (**a**) side view; (**b**) top view.

2.2. Experimental Results

Figure 6 shows the overlay of FRFs measured in configuration 1. The modulus plot highlights the presence of the fundamental mode at about 13 Hz, and the phase plot corroborates this fact, showing large phase changes at the same frequency.
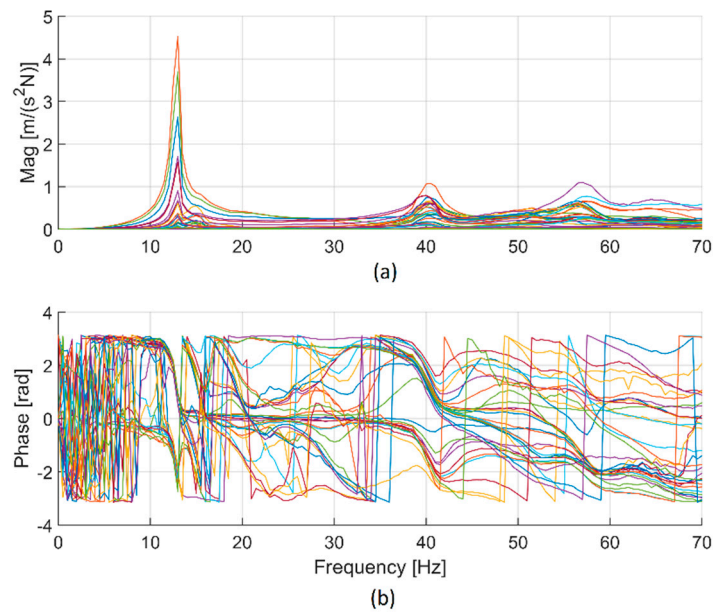
Figure 6. FRFs measured in the first test configuration (modulus (**a**) and phase (**b**)).

The identification, carried out with the algorithm Quick Fit of ModalVIEW, made it possible to find a natural frequency of 13.0 Hz, with a viscous damping ratio [26] of 2.3%. The natural frequency is the main parameter needed to identify the stiffness of the joint, but the shape of the identified mode is important as well, since it makes possible the verification of the hypothesis that the selected joint dominates the mode of vibration. The mode of vibration corresponding to the natural frequency of 13.0 Hz is represented in Figure 7; it is dominated by displacements in the x–y plane caused by the rotation of joint 1, and the contribution of the other joints and of link flexibility to this mode appears negligible. Therefore, the identified frequency is suited to identify the stiffness of joint 1.
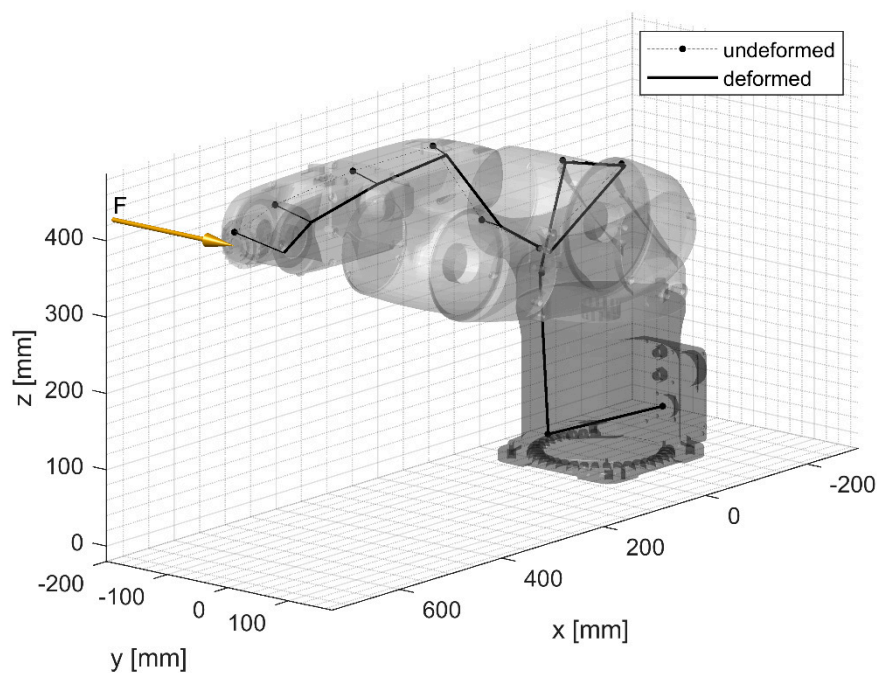

Figure 7. Mode at 13.0 Hz for the identification of joint 1 compliance.

The small resonance peaks at about 40 and 57 Hz in Figure 6 are related to the excitation of higher-order modes that also involve the compliance of the other joints of the robot.

The results of the modal tests carried out in order to identify the compliance of joint 2 are presented in Figures 8 and 9. The overlay of the measured FRFs shows the first peak at about 18 Hz. Modal analysis made it possible to identify a mode of vibration with natural frequency 17.5 Hz and viscous damping ratio of 1.9%. The shape of this mode of vibration (Figure 9) is characterized by displacements dominated by the rotation of joint 2, therefore it is suited to identify the compliance of this joint.
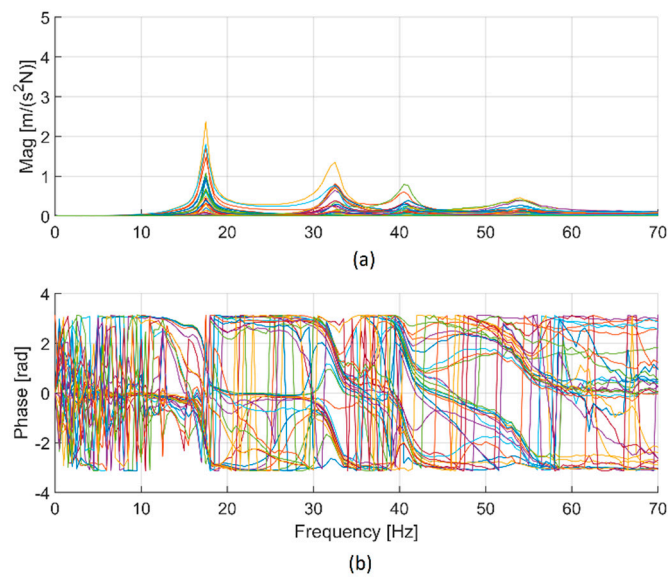

Figure 8. FRFs measured in the second test configuration (modulus (**a**) and phase (**b**)).
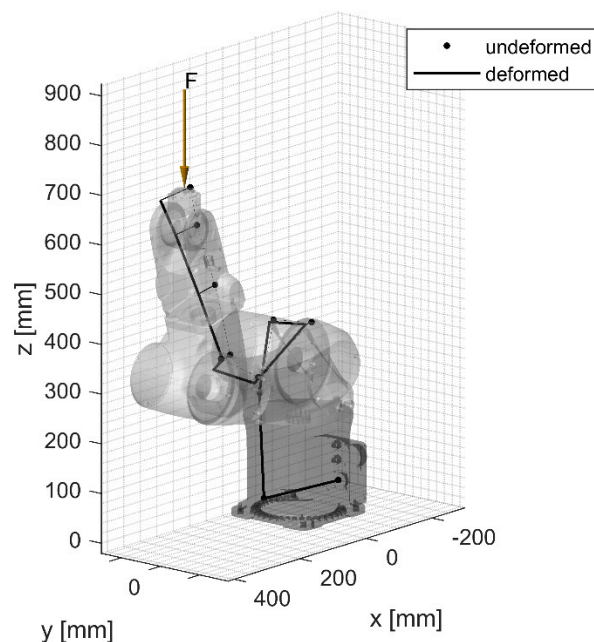

Figure 9. Mode at 17.5 Hz for the identification of joint 2 compliance.

The minor resonance peaks at about 32 and 40 Hz are related to the excitation of higher-order modes that also involve the compliance of the other joints of the robot.

Finally, Figure 10 shows the FRFs measured in the third configuration, in order to identify the compliance of joint 3. Two resonance peaks appear. The first is at about 14 Hz and the second, which is the highest, is at about 33 Hz. Modal analysis results show that the first peak (the minor) corresponds to a mode dominated by the compliance of joint 2; this mode was excited since the hammer force did not intersect exactly the axis of joint 2. The mode at 33.5 Hz (with viscous damping ratio of 2.7%) is dominated by joint 3 compliance and is suited to identify the compliance of this joint (see Figure 11).

It is worth noticing that the damping ratios of the selected modes are similar; this is a good clue that highlights that these modes chiefly involve the joints, which have similar transmissions and servos that are characterized by similar dissipation phenomena.
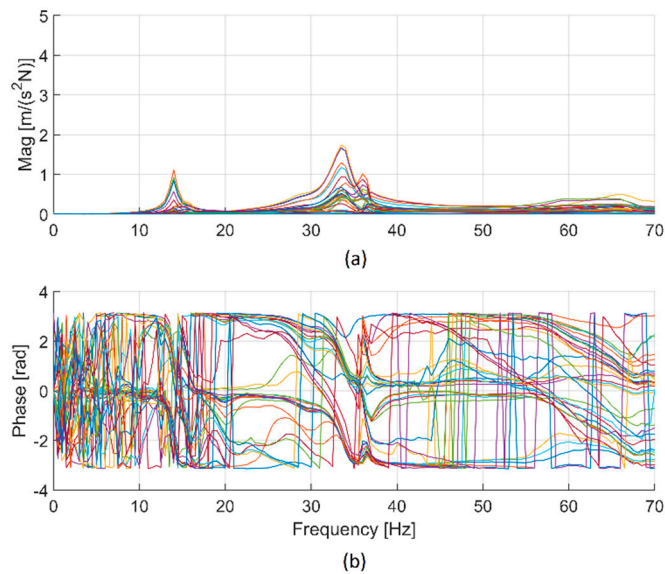

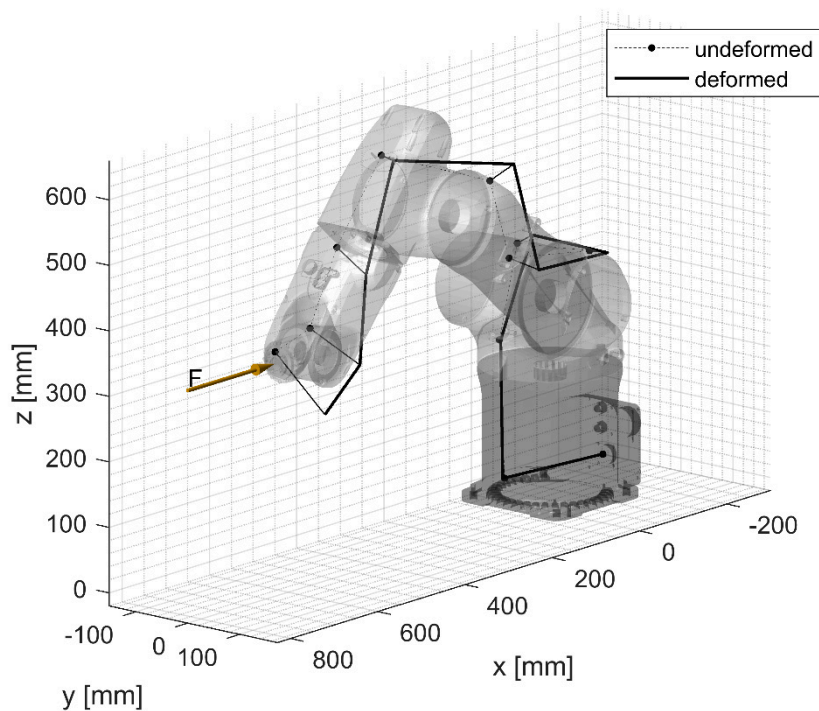**Figure 10.** FRFs measured in the third test configuration (modulus (**a**) and phase (**b**)).

Figure 11. Mode at 33.5 Hz for the identification of joint 3 compliance.

A linear vibrating system with N DOF is described by a system of coupled second-order differential equations in space coordinates. The modal approach transforms the N DOF vibrating system into N independent 1-DOF vibrating systems [20,27] governed by these equations:

$$m_k \ddot{\eta}_k + c_k \dot{\eta}_k + k_k \eta_k = F_k(t) \quad k = 1 \ldots N \tag{2}$$

where m_k, c_k, k_k are the modal mass, damping, and stiffness, respectively. η_k is the kth modal coordinate and $F_k(t)$ is the modal force. The natural frequency is:

$$\omega_k = \sqrt{\frac{k_k}{m_k}} \tag{3}$$

If robot vibrations are considered, in general, modal stiffness does not coincide with joint stiffness, because the modes of vibration involve rotation about several joints. However, if a mode i exists that is dominated by rotation about joint i, the modal stiffness k_i is a good approximation of joint stiffness kq_i. Therefore, joint stiffness can be calculated from Equation (3) with $k = i$. In this case, modal mass m_i coincides with the moment of inertia of the robot about joint i. These moments of inertia were calculated using the CAD model of the robot.

Since the manufacturer gives the total mass of the robot (28 kg) but does not give information about mass distribution, the total volume of the robot and of the various links were carefully calculated and the total mass was distributed to the links proportionally to their volumes. In the future, the calculated values will be checked with other methods.

The stiffnesses identified with the above-mentioned method are summarized in Table 2; they are similar for the three joints and in agreement with literature values [13].

Table 2. Identified parameters.

Joint	Configuration	Natural Frequency [Hz]	Moment of Inertia [kgm²]	Stiffness [Nm/rad]	Compliance [rad/(Nm)]
1	Test 1	13.0	1.990	12913	7.74×10^{-5}
2	Test 2	17.5	0.809	9738	1.03×10^{-4}
3	Test 3	33.5	0.229	10240	9.76×10^{-5}

2.3. Validation

In order to assess the validity of the identification method, the stiffness values of Table 2 were implemented in a dynamic model of the robot and the first natural frequencies of the robot were calculated in a configuration (validation configuration) different from the configurations used for identification (see Table 1 and Figure 12).

Then, the robot was modally tested in the validation configuration and the first natural frequencies were experimentally identified. Hammer excitation was applied on the end-effector along three orthogonal directions of the end-effector coordinate system. It is worth noticing that the validation configuration was chosen in order to obtain modes of vibration that involved the compliance of various joints simultaneously.
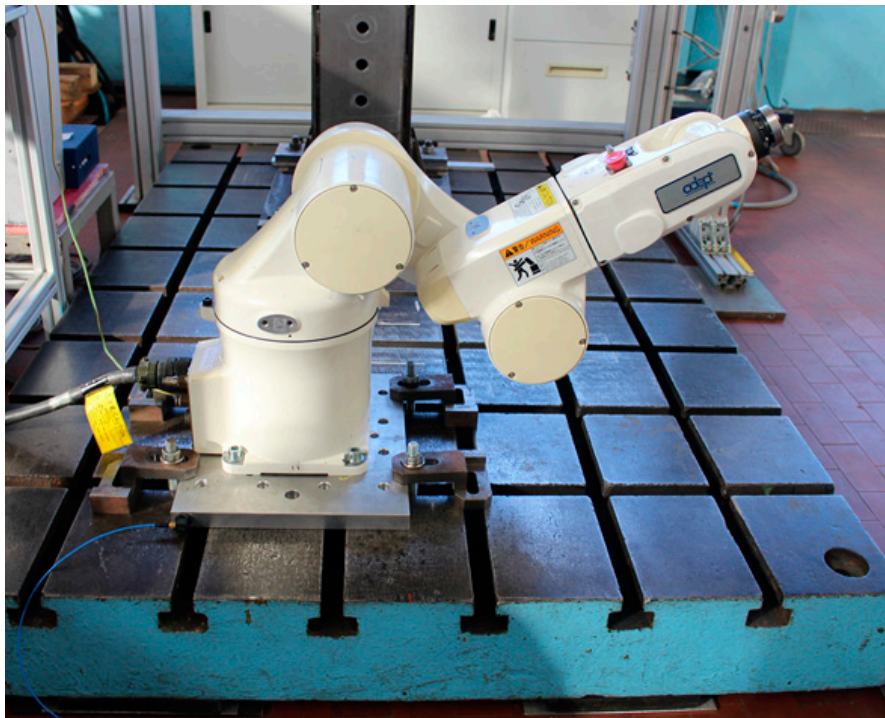
Figure 12. Robot configuration for validation.

The comparison between numerical and experimental values is shown in Table 3. The three testing conditions (with different directions of excitation) essentially lead to the identification of the same natural frequencies. These frequencies are rather close to the numerical ones, with a maximum error of about 3 Hz in the natural frequency of the third mode.

Table 3. Validation tests.

Natural Frequency	Experimental x Excitation [Hz]	Experimental y Excitation [Hz]	Experimental z Excitation [Hz]	Numerical [Hz]
1	16.0	16.0	16.0	15.0
2	-	18.0	17.5	16.5
3	37.0	36.5	35.5	39.0

3. Mathematical Model

When a structure (like a robot) has a polygonal open shape with an end locked to a very stiff structure and an end loaded by a static or dynamic force, the deformation of the loaded end can be studied considering the motion of a rigid body fixed to the loaded end of the structure. The basic concepts of rigid body mechanics can be adopted for describing this motion.

Giulio Giuseppe Mozzi del Garbo was an Italian mathematician who published in 1763 the book "Discorso matematico sopra il rotolamento dei corpi" (Mathematic Discourse on the Roll of Bodies) in which he stated that a generic differential spatial rigid motion can be considered a helical motion around a line, which is called the Mozzi axis [27]. In other words, the rigid motion of a body is represented in every instant by rotation about and translation along the Mozzi axis, which is also known as the instantaneous screw axis. The direction of the Mozzi axis coincides with the instantaneous direction of the angular velocity vector. Afterwards, the ideas of Mozzi were developed by Cauchy in 1827, Poinsot in 1834, Chasles in 1878 [28]. Ball in 1900 developed the modern screw theory introducing the concepts of twist and wrench [29,30]. A twist is the combination of a screw with a parallel linear velocity related to the angular velocity by the pitch of the screw; a wrench is a force acting along the screw combined with a torque related to the force by the pitch of the screw.

In recent years, the interest in the screw theory increased due to the discovery of possible applications in the fields of multibody dynamics [31], vehicle dynamics [32–34], vibration control [35], and robotics. In robotics, the screw theory has been adopted for calculating Jacobians [18], for decomposing the stiffness matrix [36], and for finding its properties [37,38]: the twist-compliant axes and the wrench-compliant axes. A twist about a twist-compliant axis produces only a torque parallel to the rotation axis, whereas a wrench applied on a wrench-compliant axis produces a parallel linear deformation.

In the framework of this research, the concepts of screw theory will be used for a different purpose: the representation of the rotation and translation axis of the compliant motion of the end-effector caused by an external load. This information is very useful when the robot end-effector interacts with an object and the displacement caused by compliance may assist or counteract the performed operation. Sometimes the object is characterized by its own compliance, and in the near future, the same concepts will be adopted to represent the relative rotation and translation between the robot and the object.

In order to accomplish this specific task, the basic concepts of Mozzi or screw axis are sufficient. In Figure 13, a serial six-joint robot is represented. A fixed system of coordinates with origin O_o and axes $x_o\, y_o\, z_o$ is established. Joint rotations are fixed but compliance is allowed in the first three joints. Point Q is the center of the wrist. Since wrist joints are infinitely stiff, link 3, the wrist, the end-effector, and the tool grasped by the end-effector form a unique rigid body, which is used for Mozzi axis analysis. Point O_t is used for defining the external force on the tool, which causes robot arm deformation. It is worth noticing that if the compliance of some wrist joint were important, the rigid body would begin after the last compliant joint.
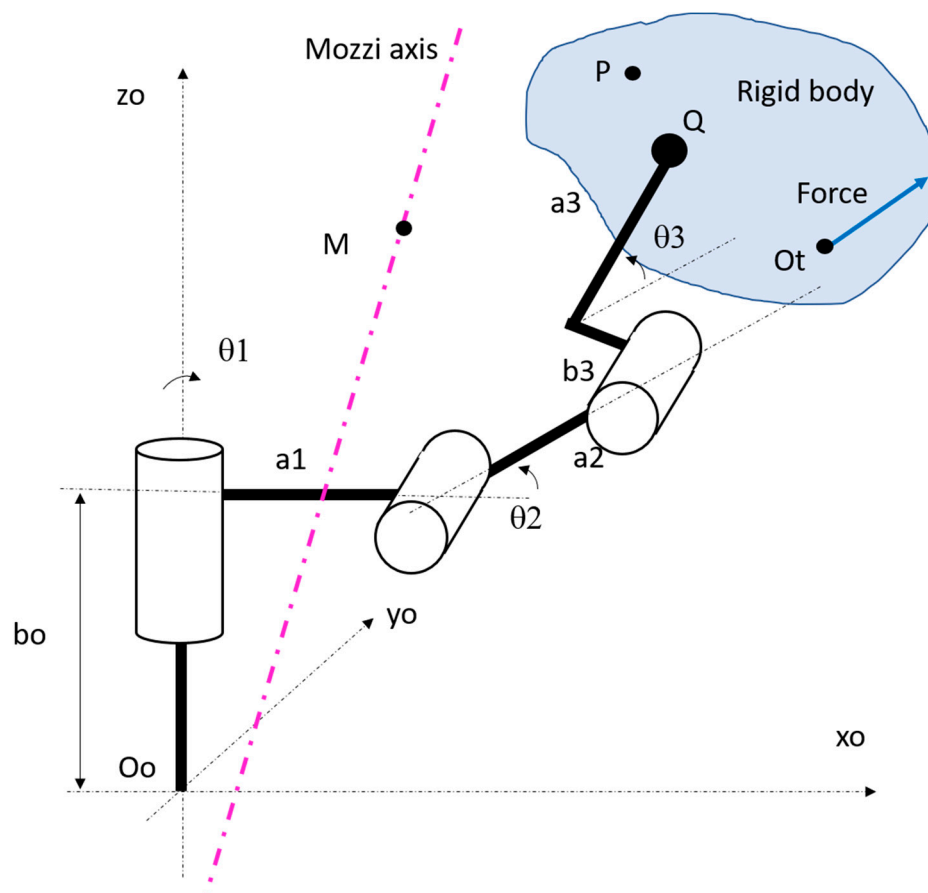

Figure 13. Kinematic model of the tested robot.

The linear velocity $\vec{v}_P$ of a point P belonging to the rigid body can be calculated using the equation of rigid body velocity:

$$\vec{v}_P = \vec{v}_Q + \vec{\omega} \times \vec{QP} \tag{4}$$

where $\vec{v}_Q$ is the linear velocity of a reference point belonging to the rigid body (wrist center Q), $\vec{\omega}$ is the angular velocity vector, and $\vec{QP}$ is the vector from Q to P.

The linear velocity of point P can be expressed as a translation along the Mozzi axis plus a rotation about the Mozzi axis according to this equation:

$$\vec{v}_P = k\vec{\omega} + \vec{\omega} \times \vec{MP} \tag{5}$$

where k is a scalar and M is a point on the Mozzi axis. If the two expressions of $\vec{v}_P$ are equated, the following result holds:

$$\vec{v}_Q + \vec{\omega} \times \vec{QM} = k\vec{\omega} \tag{6}$$

Velocity $\vec{v}_Q$ in general has a component ($\vec{v}_{Q\parallel}$) parallel to $\vec{\omega}$ and a component ($\vec{v}_{Q\perp}$) perpendicular to $\vec{\omega}$, whereas the vector product is always perpendicular to $\vec{\omega}$. Hence Equation (6) splits into the two equations:

$$\vec{v}_{Q\perp} + \vec{\omega} \times \vec{QM} = 0 \tag{7}$$

$$\vec{v}_{Q\parallel} = k\vec{\omega} \tag{8}$$

The parallel component $\vec{v}_{Q\parallel}$, which coincides with the linear velocity along the Mozzi axis, can be calculated by means of the inner product:

$$\vec{v}_{Q\parallel} = \vec{\omega} \cdot \vec{v}_Q \frac{\vec{\omega}}{|\omega|} \tag{9}$$

where $\frac{\vec{\omega}}{|\omega|}$ is the unit vector of $\vec{\omega}$. The perpendicular component ($\vec{v}_{Q\perp}$) can be calculated by difference:

$$\vec{v}_{Q\perp} = \vec{v}_Q - \vec{v}_{Q\parallel} \tag{10}$$

Moreover, for the perpendicular component, this equation holds:

$$\vec{\omega} \cdot \vec{v}_{Q\perp} = 0 \tag{11}$$

The unknown of the system of Equations (7) and (11) is vector $\vec{QM}$, which defines the position of a point on the Mozzi axis. Since the angular velocity matrix is skew-symmetric [18], there are infinite solutions for $\vec{QM}$ that belong to a line; this line is the Mozzi axis. The solution of the system of (7) and (11) can be found using vector algebra as shown in [18]:

$$\vec{QM} = \frac{\vec{\omega} \times \vec{v}_{Q\perp}}{\omega^2} + \mu\vec{\omega} \tag{12}$$

where μ is an arbitrary scalar parameter. Therefore, the position of a point along the Mozzi axis with respect to origin O_o is given by:

$$\vec{O_oM} = \vec{O_oQ} + \vec{QM} \tag{13}$$

If all the vectors are projected on the fixed coordinate system, these scalar equations define the Mozzi axis:

$$\left\{ \begin{array}{c} O_o M_x \\ O_o M_y \\ O_o M_z \end{array} \right\} = \left\{ \begin{array}{c} O_o Q_x \\ O_o Q_y \\ O_o Q_z \end{array} \right\} + \left\{ \begin{array}{c} (\omega_x \mu)/|\omega| - (\omega_z v_{Qy})/\omega^2 + (\omega_y v_{Qz})/\omega^2 \\ (\omega_y \mu)/|\omega| + (\omega_z v_{Qx})/\omega^2 - (\omega_x v_{Qz})/\omega^2 \\ (\omega_z \mu)/|\omega| - (\omega_y v_{Qx})/\omega^2 + (\omega_x v_{Qy})/\omega^2 \end{array} \right\} \tag{14}$$

When an interval of time *dt* is considered, Equation (14) can be written in terms of differential displacements (dQ_x, dQ_y, dQ_z) and rotations $(d\theta_x, d\theta_y, d\theta_z)$:

$$\left\{ \begin{array}{c} O_o M_x \\ O_o M_y \\ O_o M_z \end{array} \right\} = \left\{ \begin{array}{c} O_o Q_x \\ O_o Q_y \\ O_o Q_z \end{array} \right\} + \left\{ \begin{array}{c} (d\theta_x \mu)/|d\theta| - (d\theta_z dQ_y)/d\theta^2 + (d\theta_y dQ_z)/d\theta^2 \\ (d\theta_y \mu)/|d\theta| + (d\theta_z dQ_x)/d\theta^2 - (d\theta_x dQ_z)/d\theta^2 \\ (d\theta_z \mu)/|d\theta| - (d\theta_y dQ_x)/d\theta^2 + (d\theta_x dQ_y)/d\theta^2 \end{array} \right\} \tag{15}$$

When differential displacements (dQ_x, dQ_y, dQ_z) and rotations $(d\theta_x, d\theta_y, d\theta_z)$ are calculated by means of Equation (1), Equation (15) can describe the Mozzi axis of a robot with a certain configuration and an assigned force vector $\{F\}$.

The representation of the compliance properties of the robot arm by means of the Mozzi axis has some advantages with respect to the representation based on the Cartesian stiffness matrix. First, the Mozzi axis gives a more intuitive and geometric interpretation of the phenomenon. Second, the Mozzi axis also suggests the origin of the compliance, since its proximity to a joint axis identifies this axis as the most compliant.

4. Mozzi Axis of the Tested Robot

To show the potentialities of the Mozzi axis approach, multiple simulations, in two different scenarios, A and B, were performed. Both A and B configurations were excited by grinding forces along x_0, y_0, and z_0 axes. The two configurations differed in the orientation of the grinding equipment. From a generic point of view, these configurations show how the Mozzi axis changes with a different position of the grinding forces with the same robot joint configuration. Finally, a real case machining scenario [5] was simulated (Figure 14).
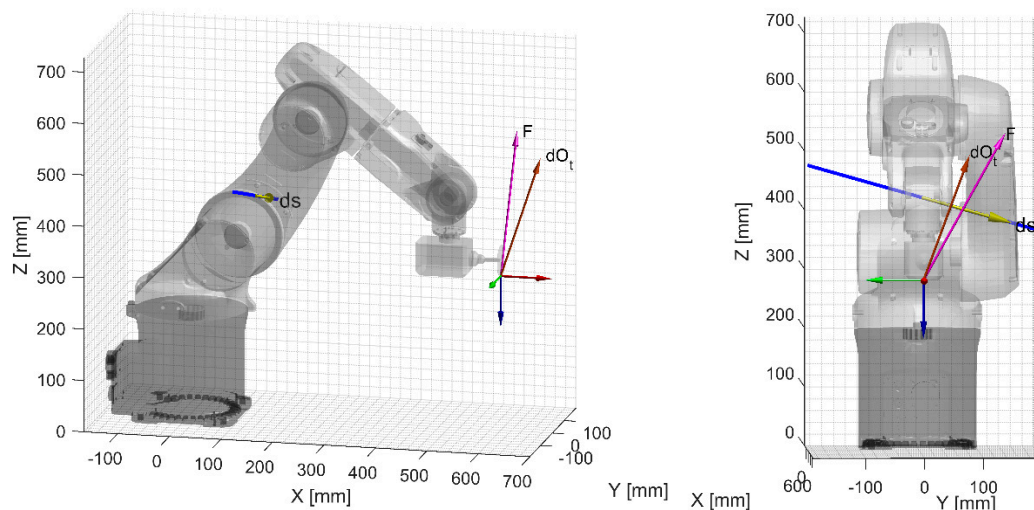
Figure 14. Configuration A excited by a machining force $\overrightarrow{F}$ applied on a plane parallel to y_0-z_0 plane, two different points of view.

In Figures 15–17, the robot is excited by a machining force that lies in the vertical plane perpendicular to the axes of joints 2 and 3. The rotation vector of the end-effector is parallel to

the axes of joints 2 and 3, therefore the Mozzi axis has the same direction and passes at a distance from the robot base that depends on the compliances of joints 2 and 3. No translation along the Mozzi axis takes place. It is worth noticing that, since in Figure 15 the force has a small lever arm with respect to joint 2, the motion of the end-effector is dominated by compliance of joint 3 and the Mozzi axis passes very close to the center of this joint. In Figures 16 and 17, the vertical force exerts moments about both joint 2 and 3 and the Mozzi axis crosses the robot at an intermediate point.
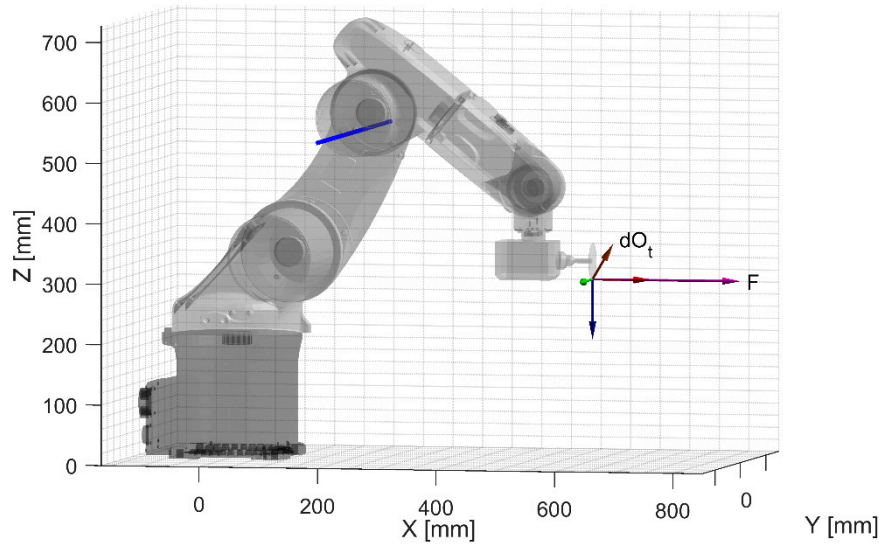
Figure 15. Configuration A with force $\vec{F}$ applied parallel to x_0 axis.
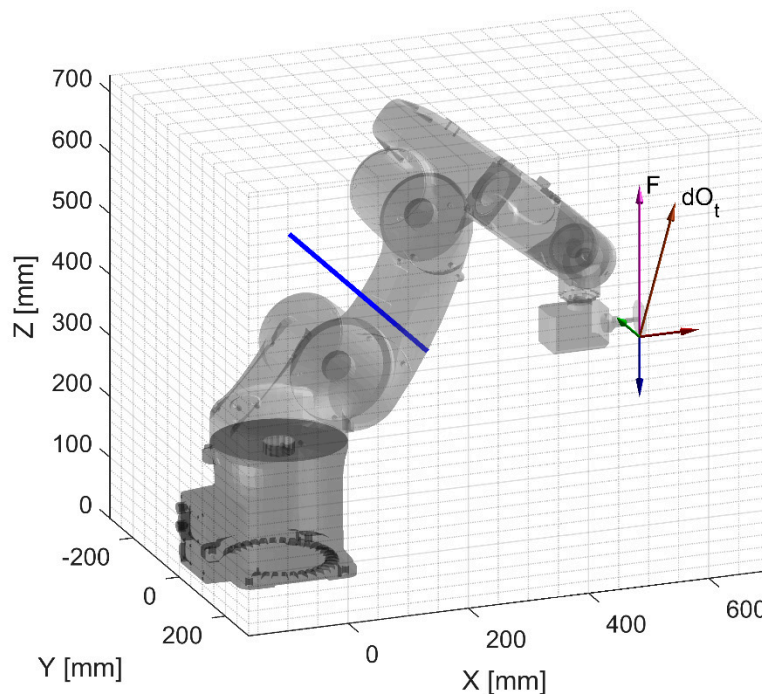
Figure 16. Configuration A with force $\vec{F}$ applied parallel to z_0 axis, bottom view.
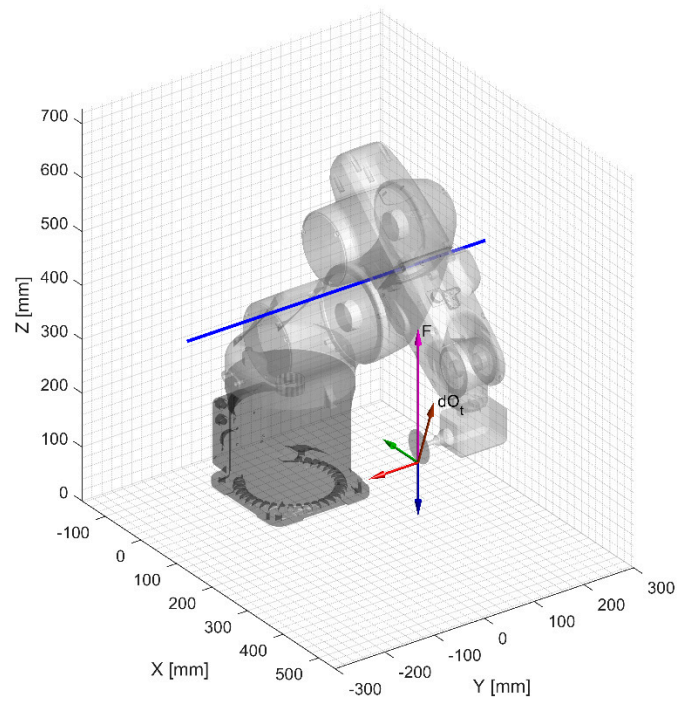
Figure 17. Configuration B with force $\vec{F}$ applied parallel to z_0 axis.

In Figures 18 and 19, the robot is excited by machining forces parallel to the y_0 axis. Since this axis is parallel to the joint 2 and 3 axes, the only joint that can comply to the machining force is joint 1, therefore the Mozzi axis is coincident with the axis of joint 1.
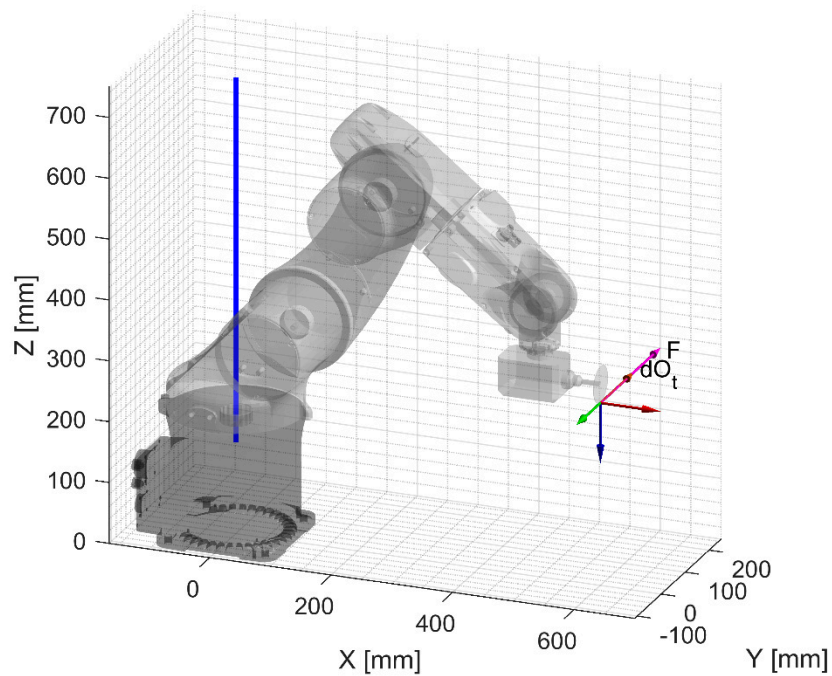

Figure 18. Configuration A with force $\vec{F}$ applied parallel to y_0 axis.
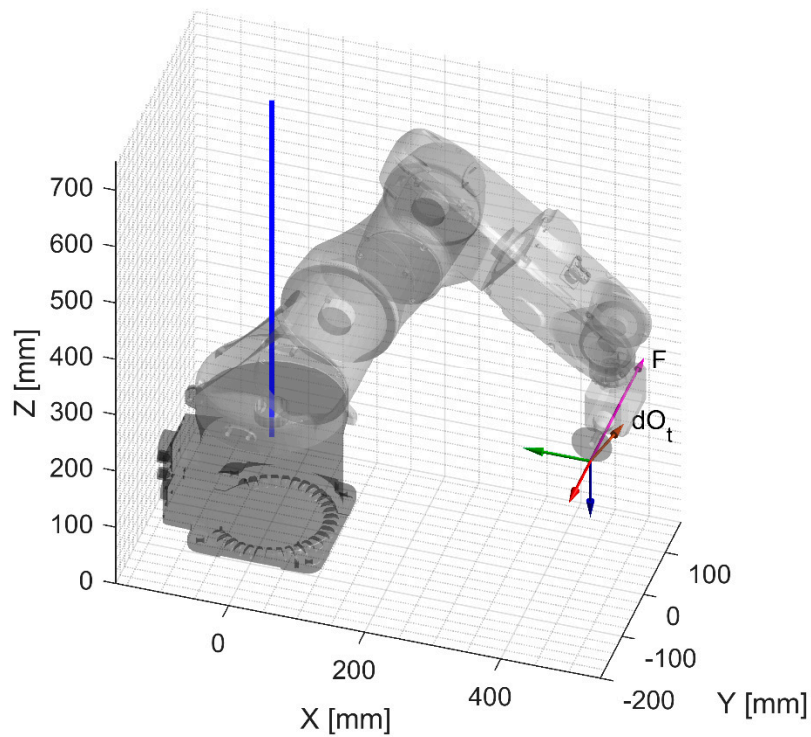
Figure 19. Configuration B with force $\vec{F}$ applied parallel to y_0 axis.

Figure 20 shows how the compliances of all the joints can combine together when excited by an eccentric force. Force $\vec{F}$ is applied parallel to the x_0 axis on a plane perpendicular to the axes of joints 2 and 3, which does not intersect the axis of joint 1. Thus, it excites all the joints and the position of the Mozzi axis results from the combination of all joint compliances. The Mozzi axis is tilted with respect to plane x_0–y_0, and there is a displacement $\vec{ds}$ along the axis as well.
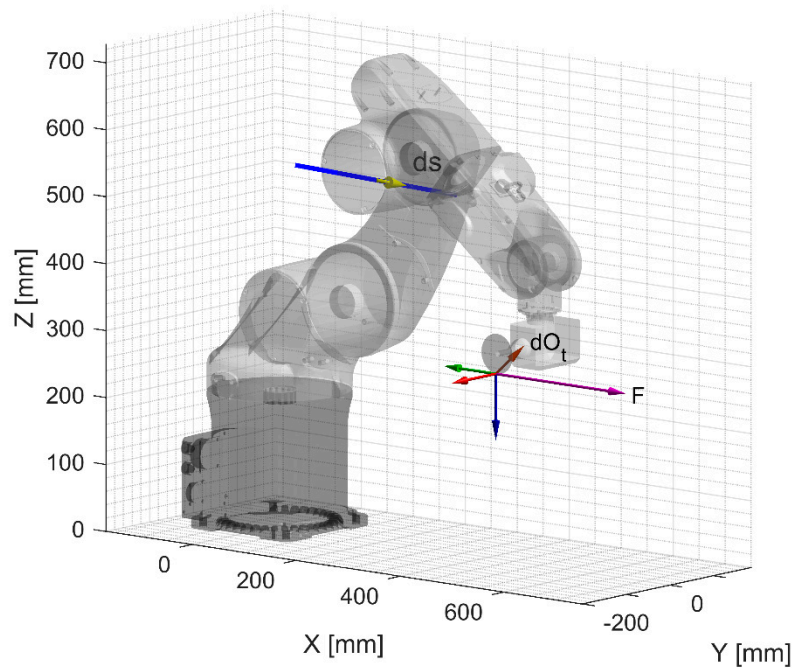

Figure 20. Configuration B with force $\vec{F}$ applied parallel to x_0 axis.

In Figure 14, a real scenario simulation is shown. Force $\vec{F}$ lies on a plane parallel to the y_0–z_0 plane and its direction is defined by the downmilling process described in [5]. In this case, the Mozzi axis has a location similar to the one in Figure 20: the main contribution to the end-effector movement is provided by the compliance of joints 2 and 3, but a small component of force $\vec{F}$ along the y_0 axis results in a non-negligible compliance of joint 1. It is interesting to notice how the high lever arm with respect to joint 1 results in a significant compliance even with a small exciting force.

Another important aspect that can be highlighted by the seven figures is the direction of the Cartesian movement $\vec{dO_t}$ of the point of application of the force. This direction is perpendicular to the Mozzi axis when displacement $\vec{ds}$ along the axis is null and a combination of both rotational and sliding displacements in the general case. Moreover, the direction is not related to the direction of force $\vec{F}$, but it depends on the compliance of the joints. The only relation that can be found between the two vectors is that this movement $\vec{dO_t}$ is placed within the semispace defined by force vector $\vec{F}$.

5. Conclusions

In this paper, two critical issues related to the compliance of industrial robots have been addressed. The first part of the paper has shown that a modal approach based on the selective excitation of some modes of vibration is a valid alternative to static tests for the identification of joint compliances. The second part of the paper has shown that the Mozzi axis of the end-effector of a robot in a certain configuration and with a certain load gives direct and concise information about the location and direction of rotational and linear compliance.

These results have been obtained dealing with a serial six-joint robot with three compliant joints. In the near future, the analysis will be extended to other types of robots with a larger number of joints. The concept of Mozzi axis will be used to explore the possibility of improving the stiffness of a redundant robot in a specific task choosing appropriate configurations of the arm.

Conflicts of Interest: The authors declare no conflict of interest.

References

1. Chen, H.; Dong, F. Robot machining: Recent development and future research issues. *Int. J. Adv. Manuf. Technol.* **2013**, *66*, 1489–1497. [CrossRef]
2. Rosati, G.; Faccio, M.; Carli, A.; Rossi, A. Fully flexible assembly systems (F-FAS): A new concept in flexible automation. *Assembly Autom.* **2013**, *33*, 8–21. [CrossRef]
3. Rosati, G.; Faccio, M.; Finetto, C.; Carli, A. Modelling and optimization of fully flexible assembly systems (F-FAS). *Assembly Autom.* **2013**, *33*, 165–174. [CrossRef]
4. Faccio, M.; Bottin, M.; Rosati, G. Collaborative and traditional robotic assembly: A comparison model. *Int. J. Adv. Manuf. Technol.* **2019**, *102*, 1355–1372. [CrossRef]
5. Pan, Z.; Zhang, H.; Zhu, Z.; Wang, J. Analysis of robotic machining process. *J. Mater. Process. Technol.* **2006**, *173*, 301–309. [CrossRef]
6. Gasparetto, A. Eigenvalue analysis of mode-coupling chatter for machine-tool stabilization. *J. Vib. Control.* **2001**, *7*, 181–197. [CrossRef]
7. Gasparetto, A. A system theory approach to mode coupling chatter in machining. *J. Dyn. Syst. Meas. Contr.* **1998**, *120*, 545–547. [CrossRef]
8. Zhang, H.; Wang, J.; Zhang, G.; Gan, Z.; Pan, Z.; Cui, H.; Zhu, Z. Machining with flexible manipulator: Toward improving robotic machining performance. In Proceedings of the IEEE/ASME International Conference on Advanced Intelligent Mechatronics, Monterey, CA, USA, 24–28 July 2005.

9. Carbone, G. Stiffness analysis and experimental validation of robotic systems. *Front. Mech. Eng. Chin.* **2011**, *6*, 182–196.

10. Ni, H.; Zhang, C.; Hu, T.; Wang, T.; Chen, Q.; Chen, C. A dynamic parameter identification method of industrial robots considering joint elasticity. *Int. J. Adv. Rob. Syst.* **2019**, *16*, 1729881418825217. [CrossRef]

11. Dumas, C.; Caro, S.; Garnier, S.; Furet, B. Joint stiffness identification of six-revolute industrial serial robots. *Rob. Comput. Integr. Manuf.* **2011**, *27*, 881–888. [CrossRef]

12. Abele, E.; Weigold, M.; Rothenbücher, S. Modeling and identification of an industrial robot for machining applications. *CIRP Ann.* **2007**, *56*, 387–390. [CrossRef]

13. Rafieian, F.; Liu, Z.; Hazel, B. Dynamic model and modal testing for vibration analysis of robotic grinding process with a 6DOF flexible-joint manipulator. In Proceedings of the International Conference on Mechatronics and Automation, Changchun, China, 9–12 August 2009.

14. Alici, G.; Shirinzadeh, B. Enhanced stiffness modeling, identification and characterization for robot manipulators. *IEEE Trans. Rob.* **2005**, *21*, 554–564. [CrossRef]

15. Abele, E.; Rothenbücher, S.; Weigold, M. Cartesian compliance model for industrial robots using virtual joints. *Prod. Eng.* **2008**, *2*, 339. [CrossRef]

16. Carbone, G.; Ceccarelli, M. A stiffness analysis for a hybrid parallel-serial manipulator. *Robotica* **2004**, *22*, 567–576. [CrossRef]

17. Behi, F.; Tesar, D. Parametric identification for industrial manipulators using experimental modal analysis. *IEEE Trans. Rob. Autom.* **1991**, *7*, 642–652. [CrossRef]

18. Tsai, L.-W. *Robot Analysis: The Mechanics of Serial and Parallel Manipulators*; John Wiley & Sons: New York, NY, USA, 1999.

19. Bompos, N.A.; Artemiadis, P.K.; Oikonomopoulos, A.S.; Kyriakopoulos, K.J. Modeling, full identification and control of the mitsubishi pa-10 robot arm. In Proceedings of the IEEE/ASME International Conference on Advanced Intelligent Mechatronics, Zurich, Switzerland, 4–7 September 2007.

20. Ewins, D.J. *Modal testing: Theory and Practice*; Research studies press: Baldock, Hertfordshir, UK, 1984.

21. Cossalter, V.; Doria, A.; Mitolo, L. Inertial and modal properties of racing motorcycles. *SAE Tech. Pap.* **2002**. [CrossRef]

22. Cossalter, V.; Doria, A.; Basso, R.; Fabris, D. Experimental analysis of out-of-plane structural vibrations of two-wheeled vehicles. *Shock Vib.* **2004**, *11*, 433–443. [CrossRef]

23. Verbeke, J.; Debruyne, S. Vibration analysis of a UAV multirotor frame. In Proceedings of the ISMA 2016 International Conference on Noise and Vibration Engineering, Leuven, Belgium, 19–21 September 2016.

24. Belotti, R.; Caneva, G.; Palomba, I.; Richiedei, D.; Trevisani, A. Model updating in flexible-link multibody systems. *J. Phys. Conf. Ser.* **2016**, *744*, 012073. [CrossRef]

25. Mejri, S.; Gagnol, V.; Le, T.-P.; Sabourin, L.; Ray, P.; Paultre, P. Dynamic characterization of machining robot and stability analysis. *Int. J. Adv. Manuf. Technol.* **2016**, *82*, 351–359. [CrossRef]

26. Inman, D. *Engineering Vibration*, 4th ed.; Prentice Hall: Upper Saddle River, NJ, USA, 2013.

27. Maia, N.M.M.; Silva, J.M.M. *Theoretical and Experimental Modal Analysis*; Research Studies Press: Taunton, Somerset, UK, 1997; Volume 3.

28. Marcolongo, R. Notizie sul Discorso Matematico e sulla vita di Giulio Mozzi. *Boll. Bibliografia Storia delle Sci. Mat.* **1905**, *VIII*, 1–8.

29. Shabana, A.A. *Dynamics of Multibody Systems*; Cambridge university press: Cambridge, UK, 2013.

30. Ball, R.S.A. *Treatise on the Theory of Screws*; Cambridge university press: Cambridge, UK, 1998.

31. Lipkin, H.; Duffy, J. Sir Robert Stawell Ball and methodologies of modern screw theory. *J. Mech. Eng. Sci. C* **2002**, *216*, 1–11. [CrossRef]

32. Wu, X.; Lu, Y.; Duan, X.; Zhang, D.; Deng, W. Design and DOF Analysis of a Novel Compliant Parallel Mechanism for Large Load. *Sensors* **2019**, *19*, 828. [CrossRef] [PubMed]

33. Cossalter, V.; Doria, A. Analysis of motorcycle slalom manoeuvres using the Mozzi axis concept. *Veh. Syst. Dyn.* **2004**, *42*, 175–194. [CrossRef]

34. Cossalter, V.; Doria, A. Instantaneous screw axis of two-wheeled vehicles in typical manoeuvres. *Veh. Syst. Dyn.* **2006**, *44*, 669–678. [CrossRef]

35. Doria, A.; Taraborrelli, L. The twist axis of frames with particular application to motorcycles. *J. Mech. Eng. Sci. C.* **2016**, *230*, 3026–3039. [CrossRef]

36.　Blanchet, P.; Lipkin, H. Dual Properties for Vibration Analysis Via Screw Theory. In Proceedings of the DETC'98 1998 ASME Design Engineering Technical Conferences, Atlanta, GA, USA, 13–16 September 1998.

37.　Chen, C.; Peng, F.; Yan, R.; Li, Y.; Wei, D.; Fan, Z.; Tang, X.; Zhu, Z. Stiffness performance index based posture and feed orientation optimization in robotic milling process. *Rob. Comput. Integr. Manuf.* **2019**, *55*, 29–40. [CrossRef]

38.　Patterson, T.; Lipkin, H. Structure of robot compliance. *J. Mech. Des.* **1993**, *115*, 576–580. [CrossRef]